Breathers and thermal relaxation as a temporal process: A possible way to detect breathers in experimental situations

A. A. Castrejón Pita,[a] J. R. Castrejón Pita,[b] and A. Sarmiento G.[c]
Instituto de Matemáticas, Universidad Nacional Autónoma de México, Ave. Universidad s/n, 62200 Chamilpa, Morelos, México

(Received 6 August 2004; accepted 23 February 2005; published online 27 April 2005)

Breather stability and longevity in thermally relaxing nonlinear arrays is investigated under the scrutiny of the analysis and tools employed for time series and state reconstruction of a dynamical system. We briefly review the methods used in the analysis and characterize a breather in terms of the results obtained with such methods. Our present work focuses on spontaneously appearing breathers in thermal Fermi–Pasta–Ulam arrays but we believe that the conclusions are general enough to describe many other related situations; the particular case described in detail is presented as another example of systems where three incommensurable frequencies dominate their chaotic dynamics (reminiscent of the Ruelle–Takens scenario for the appearance of chaotic behavior in nonlinear systems). This characterization may also be of great help for the discovery of breathers in experimental situations where the temporal evolution of a local variable (like the site energy) is the only available/measured data. © *2005 American Institute of Physics*. [DOI: 10.1063/1.1896265]

The possibility of detecting and characterizing spontaneously formed breathers (highly localized modes) in nonlinear arrays via the algorithms and tools from time series analysis is investigated in detail. It is found that this approach can be of great help in both tasks, especially when one is dealing with experimental situations where only a single, local variable (e.g., site energy) may be measured with the required accuracy. It also provides a way to confirm the chaotic character of the breather and to complete its dynamical description. Additionally, it is shown that spontaneous breathers in β-Fermi–Pasta–Ulam arrays may be considered as another example of the group formed by systems where three incommensurable frequencies dominate their dynamics, a reminder of the mechanism proposed by Ruelle and Takens for the onset of chaotic behavior.

I. INTRODUCTION

In the 1940s, Hopf described the bifurcation which results from the introduction of a new frequency into the dynamics of a system;[1] this work led Landau to conjecture, as a possible mechanism for the onset of turbulence, the successive destabilization of fluid modes of incommensurate frequency.[2] Accordingly, as a stress parameter of the system is increased (e.g., the Reynolds number), successive discrete frequencies appear in the Fourier power spectrum of the fluid variables along with their integer harmonic sum and difference combinations, making the system's time dependence very complex (turbulent) when many frequencies are present. In the early 1970s, Ruelle and Takens proposed that truly chaotic time dependence can result after only a few bifurcations,[3] and offered a specific mechanism by which this might occur. Subsequent work by Newhouse, Ruelle, and Takens[4] showed that, in a system with a phase-space "flow" consisting of three incommensurable frequencies, there exist arbitrarily small changes in the parameters of the system which convert the flow from a quasiperiodic, three-frequency flow to one which is chaotic.

While there are experiments showing that such systems can and do display chaotic behavior,[5] there are others and some numerical computations that fail to find chaos associated with three or more frequencies.[6] In the 1980s, Grebogi, Ott, and Yorke[7] reported the results of numerical experiments on a model system which was designed to have exactly three frequencies and in which they could easily identify periodic, two-frequency quasiperiodic, three-frequency quasiperiodic, and chaotic behavior. More important, they measured a probability for the existence of chaos as a function of the strength of the nonlinear coupling between the various modes, and found that chaos appeared to have zero measure until the coupling was almost 3/4 of the critical coupling. Further refinement of the Ruelle–Takens scenario is found in experiments carried out during the late 1980s,[8] where the transition to chaos follows this route although only a very small portion of the parameter space is occupied by chaos (the chaotic transition is via an exchange of stability between states which have phase locked to two-frequency quasiperiodicity).

Recently, it has been found that breathers do show a similar behavior,[9,10] another example where, as will be shown in the following, the number of relevant (incommensurable) frequencies involved in the chaotic dynamics is three. This is the reason to present this particular case as another example in which the chaotic behavior of the whole

[a]Present address: Atmospheric, Oceanic & Planetary Physics, Clarendon Laboratory, University of Oxford, Parks Road, Oxford OX1 3PU, UK; electronic mail: aacp@atm.ox.ac.uk
[b]Present address: The Blackett Laboratory, Imperial College, University of London, Prince Consort Rd., London SW7 2BZ, UK; electronic mail: jose.castrejonpita@imperial.ac.uk
[c]Electronic mail: ansar@matcuer.unam.mx

system is characterized by a finite and small number of incommensurable frequencies; its evolution starts with a thermal distribution of energy and moves into states where most of the energy is concentrated in a highly localized mode: a breather initially moving (and showing a quasiperiodic behavior in time), alternating with resting stages (where it looks periodic in space); after the small initial transient, the evolution will be shown to be governed by a dynamics determined by three frequencies and characterized as chaotic by the fact that its first Lyapunov exponents are positive. Eventually, the breather will decay since the system must reach equilibrium at the particular value of the temperature bath it is immersed in, a process that is consistent with its chaotic dynamics and is due to the loss of energy via bouncing at the boundaries and possible collisions while in motion with low-frequency phonons that might have survived. For the full description and details of the analysis and the roles that different modes play in harmonic, anharmonic, and mixed systems, the reader is referred to Ref. 9, and especially to Ref. 10. It must be stressed that we are using the energy in the breather as a representative variable to describe the dynamics of the whole system because it contains most of the energy present in the system and thus is much easier to measure it and follow its evolution in comparison to the energy in the other sites; we do not neglect these other sites and their dynamical influence since the breather keeps interacting with them and participating in the collective behavior at all times.

The first reference to chaotic breathers is probably that of Cretegny *et al.*,[11] where they studied the breathers that appear in a rather different Fermi–Pasta–Ulam system. The main differences are: (i) their isolated system considers periodic boundary conditions while the case analyzed in the following appears in a system with free-end boundary sites connected to a zero-temperature environment that allows for relaxation via energy dissipation at these sites; (ii) their simulations adopt as initial condition the highest frequency ($\pi-$) mode: $x_i=(-1)^i a$, where x_i is the displacement of particle i from its equilibrium position and a is its amplitude (since this is an exact solution, they add a small amount of noise to the velocities in order to destabilize the mode), while in our example, the system is initially thermalized at a chosen value for the temperature T (details in Refs. 9, 12, and 13) and then allowed to relax; (iii) their resulting breather is never at rest and propagates in general with almost the same speed (in modulus), while the breather in our example is able to move or remain at rest (as a result of the interactions with the energy remaining in the sites not directly involved in the breather). It must be mentioned that according to Ref. 10, boundary conditions do not strongly affect equilibrium properties but do affect relaxation dynamics.

The finding of very similar mechanisms for some of the main general evolutionary paths, those which are present in the two types of system just mentioned (each type distinguished by the main differences mentioned earlier), shows that breathers are quite robust structures that appear spontaneously and are really ubiquitous, chaotic modes.

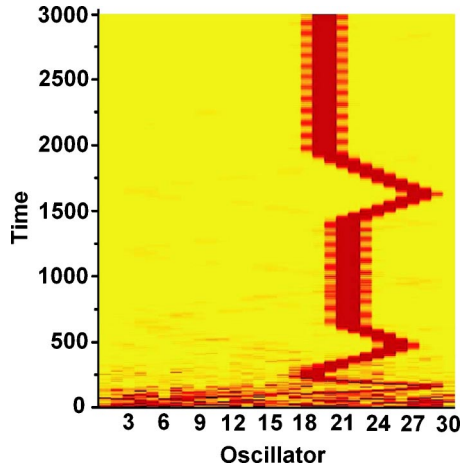

FIG. 1. (Color online) Energy landscape of 30-site mixed relaxing array initially thermalized at $T=0.5$. Other parameters: $k=k'=0.5$, $\gamma=0.1$. The horizontal axis indicates the position along the chain and time advances along the vertical axis from $t=0$ until $t=3000$. An intensity scale is used to represent the local normalized energy, $E(t)$ Eq. (3), with higher intensity corresponding to more energetic regions; color figure available for the online edition.

II. MODEL SYSTEM

In the present study, we shall consider the energy in each one of the oscillators in a nonlinear array as the data that represent the time series under analysis; the main reason for this selection is due to the fact that the energy is one of the most accessible variables for experimental, precise measurements. As already mentioned, we shall use the breather found in Refs. 9 and 10 for a β-Fermi–Pasta–Ulam (FPU) relaxing array with 30 oscillators and shown for a longer lapse in Fig. 1. Boundary sites are connected to a zero-temperature environment by adding dissipation terms $-\gamma\dot{x}_i$ to the equations of motion of these sites. The equations of motion are integrated using a fourth-order Runge–Kutta method with a time interval $\Delta t=5\times10^{-4}$, which assures a precision of at least ten significant figures over all time ranges reported herein; because of this small value for Δt, the fact that positions, velocities, and energies have to be stored for all sites at every step of integration (implying a considerable amount of storage for large arrays), and the fact that these highly localized modes decay exponentially in time (with comparatively enormous time constants, of the order of 10^{13-14}),[10] we are not able to follow the evolution of the breather up to its complete disappearance. Such a small Δt is necessary to obtain reliable values in the calculations; the best example is provided by the derivation of the first Lyapunov exponents (Sec. III D).

One can easily note in Fig. 1 the quick decay of long-wavelength phonons and the persistence of certain high-frequency spectral components. The harmonic part of the interaction allows the relaxation process to sweep the system clean of the excitations that most readily perturb the spontaneously created breather, making it possible for the breather to persist. Even though the spontaneous creation and further evolution of the localized mode are a consequence of the collective dynamics of the system, involving all oscillators, one can see in Fig. 1 that after the transient lapse (during

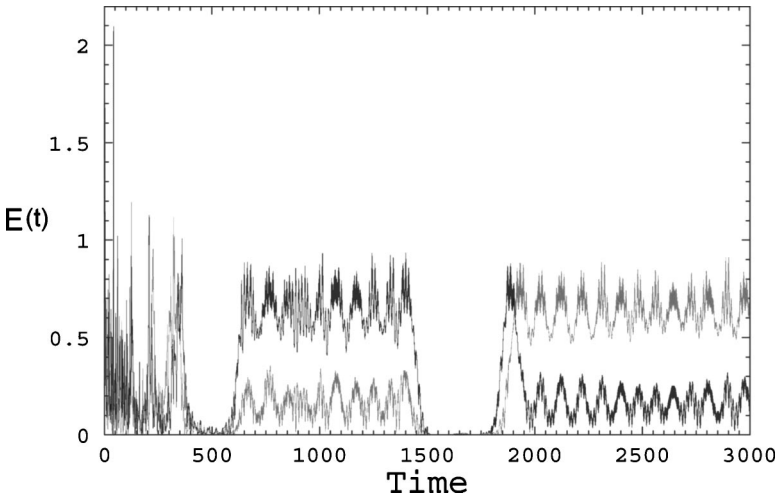

FIG. 2. Local normalized energy as a function of time for the oscillator at sites 20 (gray) and 21 (black). Note in both sites, the two stages where the localized mode stops moving: a resting breather with its corresponding oscillations containing most of the energy in the system, and the almost null (undetectable) energy that remains in these sites when the breather is in motion ($t \in [1500, 1800]$).

which some energy is lost by dissipation at the boundary sites), and once the breather is well established as a highly localized mode, there is not much energy in the sites which are not directly involved in the breather structure. This feature enables us to use the energy in the breather as the data representing the time series and asserts the validity of the tools employed in the analysis. Note, however, that even at much longer times, there are some lapses where high-frequency spectral components appear outside the breather (tenuous shadow in sites 26–28 close to the top of the figure) indicating that the rest of the system is still participating in the dynamics; it must also be recalled that while these components stay static, they do not perturb the localized mode unless the moving breather collides with them (traces of the collisions with other modes that set the breather in motion or stop it can be clearly seen in Fig. 1).

The local energy is customarily defined as

$$\epsilon_i(t) = \frac{p_i^2}{2m} + \frac{1}{2}V(x_{i+1} - x_i) + \frac{1}{2}V(x_i - x_{i-1}) \tag{1}$$

where x_i is the displacement of particle i from its equilibrium position, N is the number of sites, $V(z)$ is the FPU potential,

$$V(z) = \frac{k}{2}z^2 + \frac{k'}{4}z^4, \tag{2}$$

and k and k' are the harmonic and anharmonic force constants, respectively. In what follows, we shall consider the local normalized energy:

$$E(t) = \frac{\epsilon_i(t)}{\sum_{i=1}^{N} \epsilon_i(t)} \tag{3}$$

of a particular site and therefore we shall drop the subindex i.

In our example, the spontaneously created breather involves three oscillators while in motion (odd-parity) and four oscillators when it stops (even parity); we shall first concentrate our analysis on oscillators where the localized-energy mode stops for a certain lapse and its breathing is conspicuous; the reason for this being that it is then when one can easily apply the tools employed for time series analysis.

III. BREATHERS AT REST

There are two such situations: a first resting stage in sites 20–23 for $t \in [640, 1440]$, and a second one in sites 18–21 for $t \in [2000, 3000]$; therefore, only sites 18–23 will be analyzed. We shall also make a distinction between the two cen-

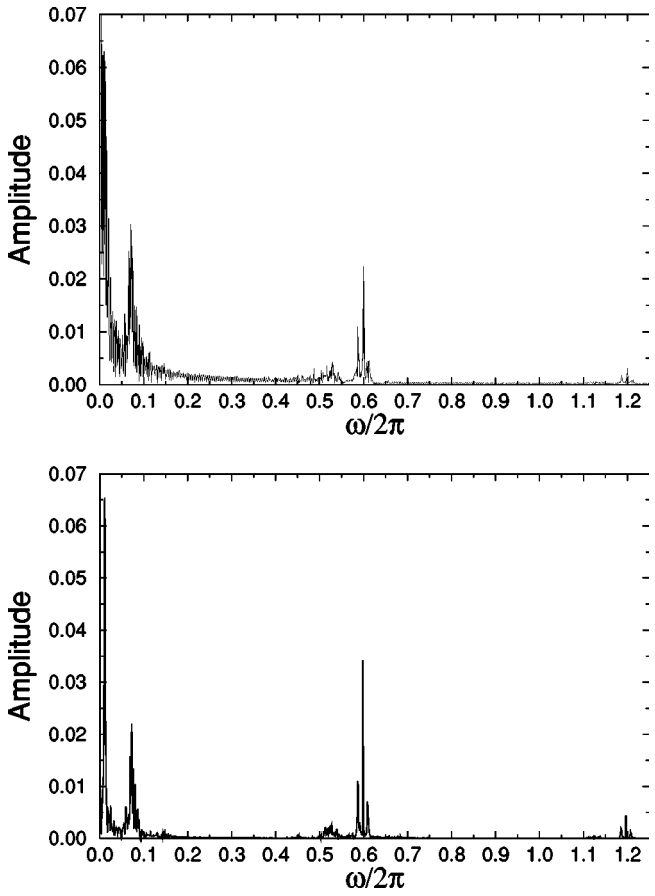

FIG. 3. Fourier transform of the time series shown in Fig. 2 for site 21 and $t \in [640, 1440]$, i.e., first resting stage of the breather, and for site 20 and $t \in [2000, 3000]$ or second resting stage; both sites are in the center of a breather. Note that for the second stage (lower panel), the intermediate frequency ($\omega_2/2\pi$) becomes less relevant than the highest one ($\omega_3/2\pi$), an interchange that takes place as the breather starts moving ($t \in [1470, 1900]$, Sec. IV).

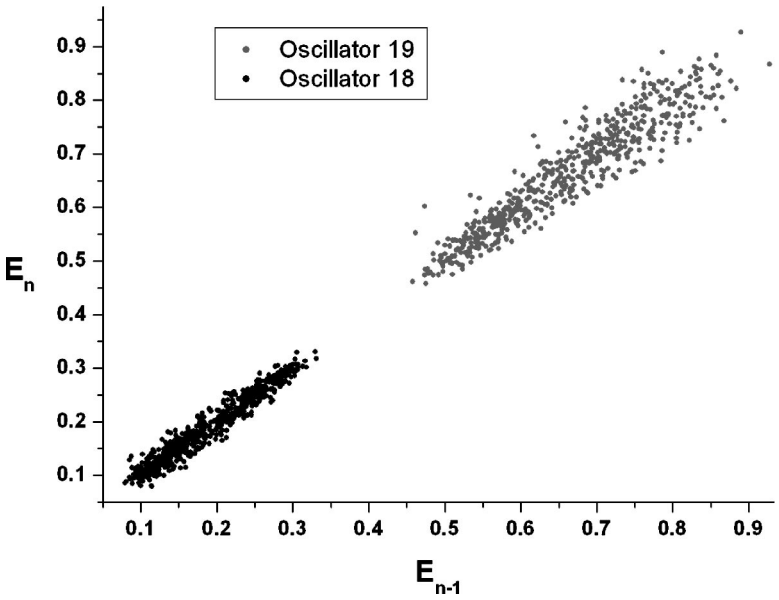

FIG. 4. Return maps for the oscillators in sites 18 (black points, lower left cluster) and 19 (gray points, upper right cluster) for $t \in [2000, 3000]$ or second resting stage. The graph shows the energy extrema in one oscillator, E_n, vs the previous extrema in the same oscillator, E_{n-1}. Note again the difference in the range for the variation of the amplitudes of central oscillators (site 19 in this case) and that for the variation of the amplitudes of adjacent oscillators (18); this difference is already present in Fig. 2.

tral oscillators that form the main body of the breather (where most of the breather energy is concentrated) and their corresponding two adjacent oscillators (where the amount of involved energy is smaller). The qualitative dynamical behavior of the central oscillators is very similar and independent of the resting stage of the breather (sites 21 and 22 in the first case and 19 and 20 in the second). The same is true for the corresponding adjacent oscillators (sites 20 and 23 for the first stage, and 18 and 21 for the second one); quantitative differences are evaluated in the following sections.

The local normalized energy as a function of time is shown in Fig. 2 for the oscillators at sites 20 and 21 which interchange their roles in the two resting stages of the breather: site 20 is an adjacent oscillator in the first stage and a central oscillator in the second one, while site 21 goes from a central oscillator in the first stage to an adjacent oscillator in the second one.

The tools used for the analysis of time series are a customary content of many present day textbooks; we use a free package designed and described by Hegger, Kantz, and Schreiber,[14] which is probably the most complete package of strategies and algorithms available.

A. Number and values of the frequencies involved in the dynamics

The easiest well-known procedure to begin the analysis is to calculate the Fourier transform of a time series to obtain the number of frequencies involved in the dynamics and their corresponding values. Figure 3 shows a typical graph of the results where one can easily detect several values; in order of relevance during the first resting stage (height in the graph), these values are: $\omega_1/2\pi=0.0122$, $\omega_2/2\pi=0.0722$, $\omega_3/2\pi$

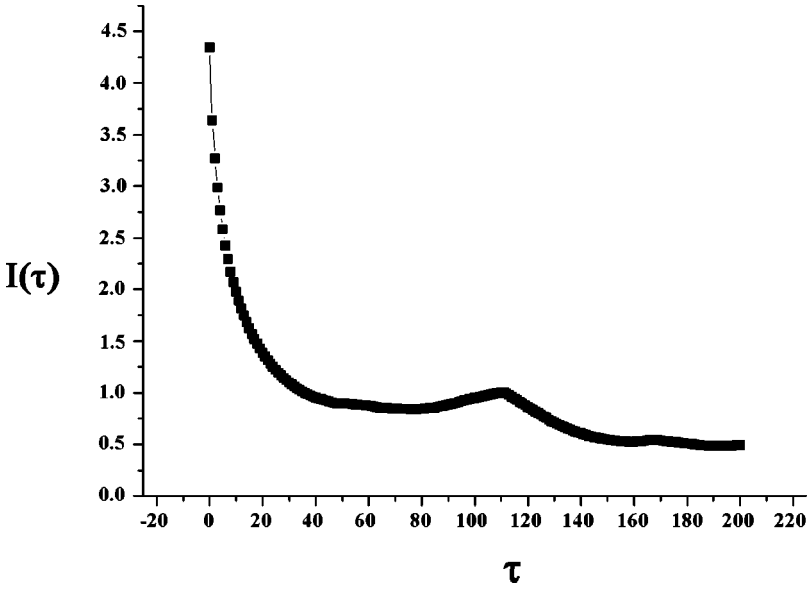

FIG. 5. Mutual information method applied to the data of the first resting stage plotted in Fig. 2, site 21. Similar results are obtained for the other oscillators involved in the main central body of the breather while it is at rest. The existence of a first minimum at $\tau \sim 50$ is easily spotted; this value will be used in reconstructing the attractor shown in Fig. 6.

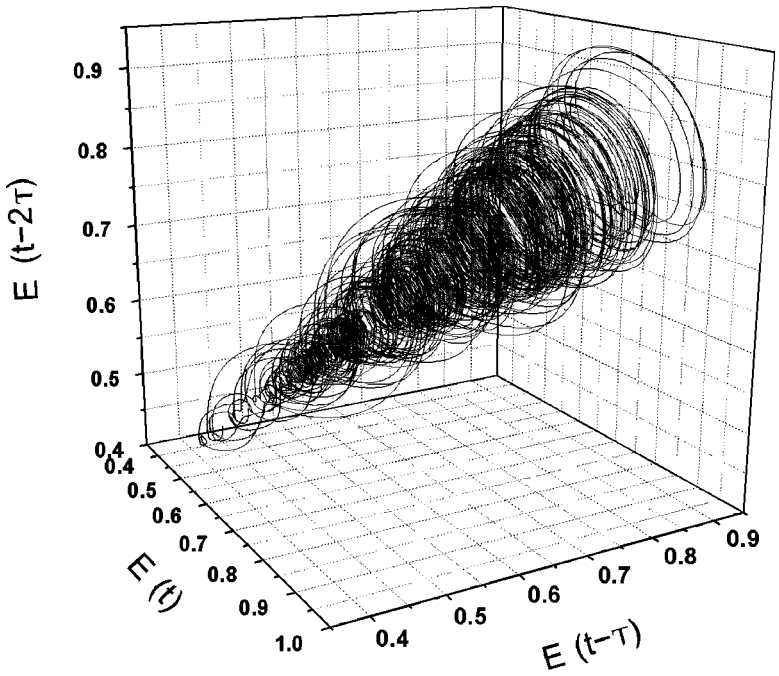

FIG. 6. Reconstructed attractor in $\mathbb{R}^3$ for $E(t)$ at site 21 and $t \in [640, 1440]$ (first resting stage, Fig. 2). The value $\tau = 50$, obtained from Fig. 5 is used for this reconstruction.

$=0.5981$, and two, much less intense values at: $\omega_4/2\pi = 0.5289$ ($\approx(\omega_3 - \omega_2)/2\pi$), and ω_3/π; all values with a precision of ± 0.0005.

From the analysis of the trajectories, one can see that during the second resting stage, for example, sites 18 and 20 oscillate in phase with a frequency $\omega_3/4\pi$, while sites 19 and 21 also oscillate in phase with the same frequency but in antiphase with the first two sites. This allows one to identify $\omega_3/2\pi$ as the frequency associated with the kinetic energy of each individual oscillator [an oscillatory motion $x(t)$ with frequency ω, has an oscillating kinetic energy $\propto \dot{x}^2(t)$ whose frequency is 2ω]. The local minima and maxima of a site's trajectory coincide with the local minima of the local normalized energy for the same site, $E(t)$, (i.e., when the site's kinetic energy is null and there is only the coupling energy of the site with its neighbors), and the local maxima of $E(t)$ occur at a time when the oscillator happens to be at the average value of its trajectory (i.e., when the site's kinetic energy attains its maximum value and the coupling energy is null since the trajectories of the breather's sites coincide at the average value).

The oscillations observed in the trajectories are also modulated by $\omega_1/2\pi$ (but now sites 18 and 19 are in phase while sites 20 and 21 are also in phase but in antiphase with respect to the first pair of sites) and only slightly by $\omega_2/2\pi$ [sites 18 and 20 (19 and 21) now oscillate with a phase

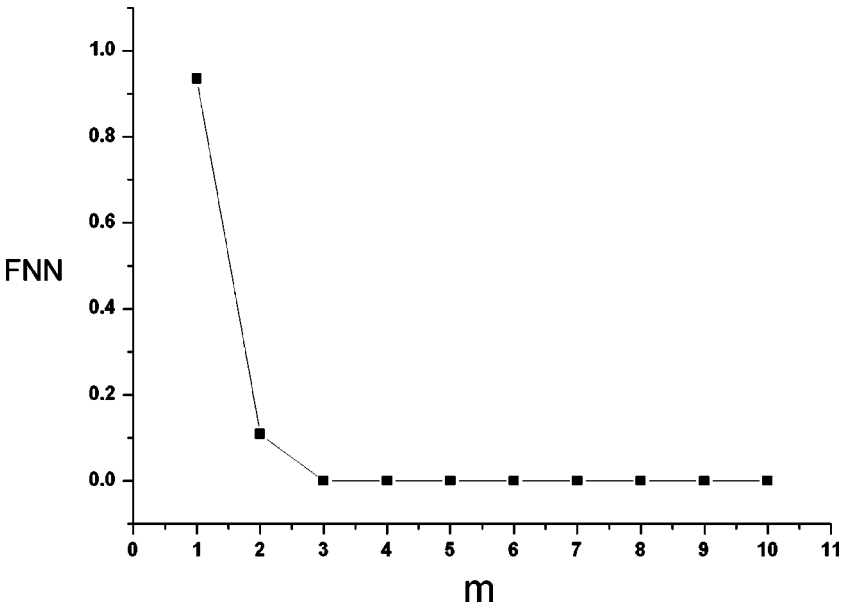

FIG. 7. Number of false neighbors as a function of the embedding dimension m for the reconstructed attractor in Fig. 6. It is clear that for $m=3$ there are already no false neighbors.

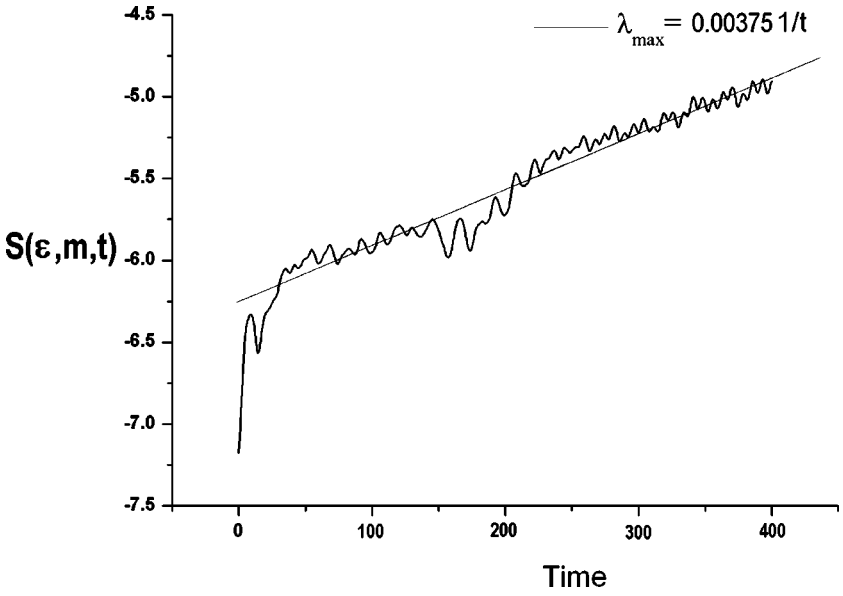

FIG. 8. Largest Lyapunov exponent for the oscillator in site 21 and $t \in [640, 1440]$, first resting stage. The value in the upper right corner is calculated according to the method mentioned in the text.

difference of π and there is also a phase difference of $\pi/2$ in the oscillations of the first pair of sites with respect to the second one].

B. Return maps

We now look for possible periodic or quasiperiodic behavior using the return map method, where the local extremal values of the time series are plotted as a function of the immediately preceding extrema. In our case, we shall plot the normalized energy extrema in an oscillator (denoted by E_n) as a function of the previous extrema in the same oscillator (E_{n-1}). The return map for oscillators 18 and 19 is shown in Fig. 4. Note that this plot agrees with Fig. 2, where one can see that a central oscillator (site 19 in the present case) has an amplitude that fluctuates between 0.5 and 1.0, approximately, while the amplitude of an adjacent oscillator (site 18) varies from 0.0 to 0.4, approximately.

Since in the case of a periodic dynamics this plot would consist of single points (whose number would indicate the periodicity of the system), we can rule out this possibility. Unfortunately, it does not seem adequate to try to use the return maps for a clear distinction between quasiperiodic dynamics (where the return map would be a simple closed curve) and probably chaotic dynamics (return map represented by an open thick curve); the data do not allow for a trusty statement. The following analysis, however, will provide a reliable answer.

TABLE I. First Lyapunov exponent.

Site No.	First stop	Second stop
19		0.000 98±0.000 11
20		0.001 42±0.000 21
21	0.003 75±0.000 09	
22	0.003 62±0.000 12	

C. Time delay graphs

We shall now devote our analysis to confirm whether our time series is periodic or not by means of the useful graphical device consisting of plotting the time series using delay coordinates. In our case, a delay-coordinate reconstruction in $\mathbb{R}^3$ means plotting each value of the time series of the local normalized energy $E(t)$ for one oscillator *versus* a time-delayed version, and a twice delayed version: $(E(t), E(t-\tau), E(t-2\tau))$, for a fixed delay time τ. If the system was to settle into a periodic state, the delay-coordinate points would fit together in a loop that would make one revolution for each oscillation in the time series, i.e., it would reproduce the periodic orbit of the true system state space. In other words, periodic motion in $\mathbb{R}^k$ means that trajectories trace out a one-dimensional curve of states through $\mathbb{R}^k$.

For nonperiodic systems, however, the problem may still involve self-intersections of the state space curve. In order to remove them, we use an m-dimensional delay plot which consists of the vector of delay coordinates $(E(t), E(t-\tau), E(t-2\tau), \ldots, E(t-(m-1)\tau))$; attractors that are more complicated than simple closed curves will require more dimensions to be untangled. In other words, we are performing a topological embedding of a compact set $E(t)$, which amounts to finding a one-to-one continuous function from the set $E(t)$ to $\mathbb{R}^m$, where m is the embedding dimension of the set. A delay-coordinate embedding means that every state of the system can be uniquely represented by the measured data because of the one-to-one property; furthermore, it can be proved that a finite-dimensional attractor can always be embedded in some $\mathbb{R}^m$ with m slightly larger than twice the dimension of the attractor.

The proper choice of the delay time τ is quite important. If it is taken too small, there is almost no difference between the different elements of the delay vectors and this redundancy makes the vectors meaningless if the data are noisy and the variation of the signal during the lapse $m\tau$ is less than the noise level. In an experimental situation, the minimum value for τ is given by the sampling rate. On the other

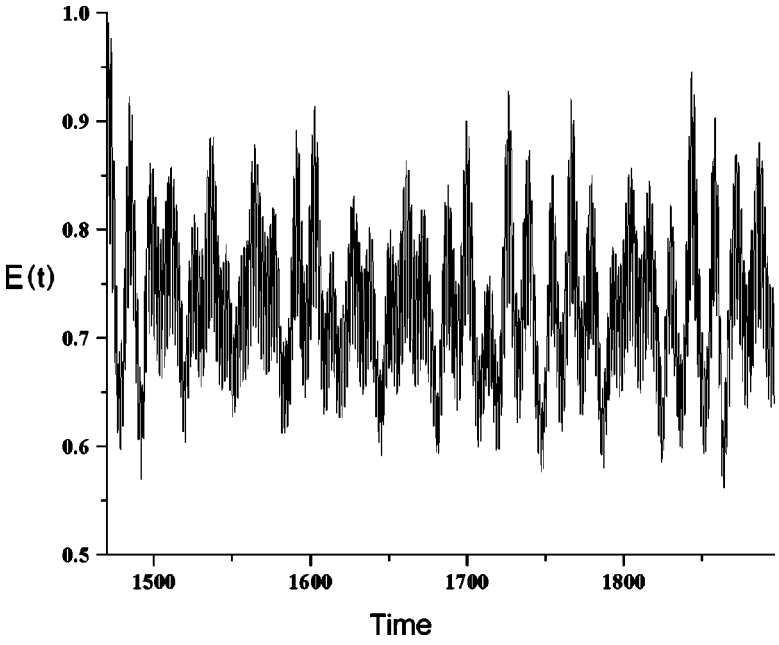

FIG. 9. Normalized energy as a function of time for the center of the breather as it moves from sites 21–22 to sites 27–28 ($t \in [1470, 1632]$), and back to sites 19–20 ($t \in [1632, 1895]$).

hand, if τ is taken too large, the different coordinates may be almost uncorrelated and the reconstructed attractor may become very complicated, even if the "true" underlying attractor is simple (typical of chaotic systems where the autocorrelation function decays fast). Unfortunately, there exists no rigorous way for determining an optimal value for τ. Most suggested methods, however, yield values of similar magnitude, and this allows one to start with an estimate and optimize its performance through variations of the initial estimate. Changing the time delay produces geometrically different but topologically equivalent sets in a delay graph and the results should not depend too sensitively on τ since, otherwise, the invariance under smooth transformations would be absent indicating that the analyzed object may not be a true attractor.

In order to choose an adequate value for τ using the time series data, we need first of all, to make sure that the attractor is unfolded, i.e., its extension in all space dimensions should be approximately the same.[14] For quantitative evaluations one has to rely on the use of statistical methods, the most natural of them being the autocorrelation function which gives hints about stationarity and typical time scales besides being intimately related to the shape of the reconstructed attractor. For our particular case, however, since this procedure is based on linear statistics and does not take into account nonlinear dynamical correlations, a better estimate will be given by the first minimum of the time delayed mutual information, regarded by some as the easiest method to get a reliable value for τ.[15]

Creating a histogram for the probability distribution of the data on the explored lapse, and denoting the probability that the signal assumes a value inside the ith bin of this histogram by p_i, and the probability that $E(t)$ is in bin i and $E(t+\tau)$ is in bin j by $p_{ij}(\tau)$; the mutual information function $I(\tau)$ is then given by

$$I(\tau) = \sum_{i,j} p_{ij}(\tau) \ln p_{ij}(\tau) - 2 \sum_{i} p_i \ln p_i. \tag{4}$$

If $\tau = 0$, the joint probabilities reduce to $p_{ij} = p_i \delta_{ij}$ and $I(\tau)$ yields the Shanon entropy of the data distribution. The value of the mutual information is independent of the particular choice of histogram if it is fine enough, and therefore, one does not need to carry an index for the bin size. In the limit of large τ, $E(t)$ and $E(t+\tau)$ have nothing to do with each other and p_{ij} factorizes to $p_i p_j$, and $I(\tau)$ becomes null. The first minimum of $I(\tau)$ marks the time delay where $E(t+\tau)$ adds maximal information to the knowledge we have from $E(t)$, or equivalently, where the redundancy is minimal. Finally, if the minimum lies at considerably larger times than the $1/e$ decay of the autocorrelation function, it is wiser to optimize τ inside this interval.

Figure 5 shows the results from the mutual information method for the first resting stage in Fig. 2, where one can read the value of $\tau \sim 50$ for the first minimum of the curve.

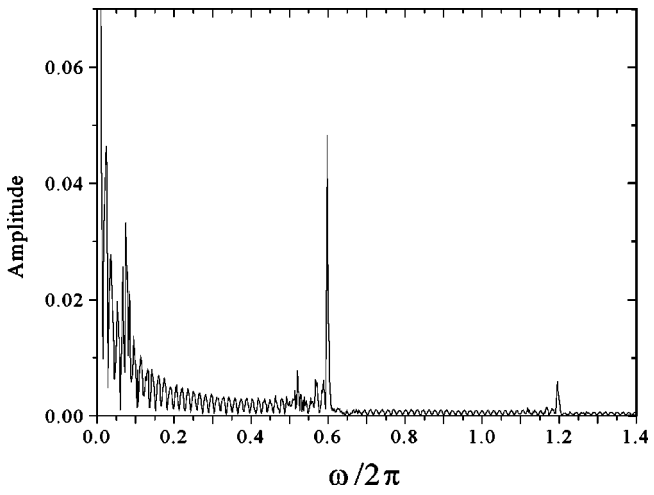

FIG. 10. Fourier transform of the time series shown in Fig. 9 for the energy in the center of the moving breather during $t \in [1400, 1650]$ (i.e., when the breather goes to the right of the array, for the second time). Compare to Fig. 3.

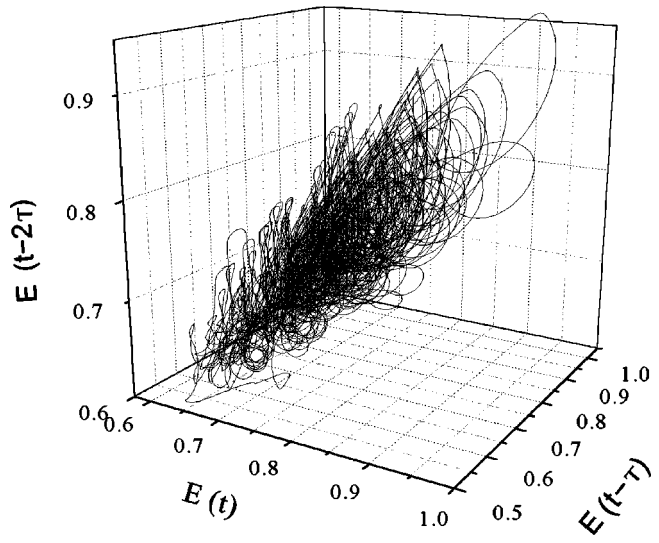

FIG. 11. Reconstructed attractor of the time series shown in Fig. 9. Compare to the attractor in Fig. 6.

In Fig. 6 we present a delay-coordinate reconstruction in $\mathbb{R}^3$ for the local normalized energy $E(t)$ in the oscillator at site 21 and $t \in [640, 1440]$ using the value for τ found in Fig. 5; reconstructed attractors of the oscillators in site 22 for the same lapse and site 19 or 20 for $t \in [2000, 3000]$ look similar. The form of the attractor shown in Fig. 6 clearly shows the dominance of the three incommensurable frequencies mentioned in Sec. I and determined in Sec. III A. It may be regarded as a cone with apex pointing left and downwards, and base close to being parallel to an $E(t-\tau)=$const plane; the highest frequency $(\omega_3/2\pi)$ is responsible for the faster motion that describes circular-like trajectories (best seen close to the base), the next frequency in decreasing order $(\omega_2/2\pi)$ governs the amplitude of these trajectories allowing for wider motion near the base, and the smallest frequency $(\omega_1/2\pi)$ controls the displacement of the circular trajectories form the base to the apex. It does not seem to be the case, but there are some dynamical systems in the literature that show attractors whose topology may be used to extract useful physical information that may be hidden in the complex dynamics of such systems; for our present case, the geometrical form of the attractor suffices to show the roles of the three dominant frequencies.

In order to test the chosen value for the embedding dimension, m, one may calculate the number of points in the trajectory that are within a certain distance from any conspicuous point or region where it is not possible to discern a self-intersection from a simple projection (these points are thus candidates to be real neighbors). One then can see if this number decreases as one increases the embedding dimension, indicating that the candidates were false neighbors and close to the conspicuous point/region due to a projection. Figure 7 clearly shows that the adequate embedding dimension is indeed three; as previously mentioned, the attractors in the other sites where a breather rests behave in a similar way and all have the same embedding dimension.

D. Lyapunov exponents

The final question on the dynamical character, quasiperiodic or chaotic behavior, will be clearly decided by the calculation of the (largest) Lyapunov exponents. This is due to the fact that any bounded trajectory, which is not asymptotically periodic and has a positive Lyapunov exponent, is a chaotic trajectory. Let us take two points in the state space, say $E(t)$ and $E(t')$, which are initially very close to each other: $|E(t)-E(t')| < \delta_0 \ll 1$, and denote the distance between the trajectories emerging from these two points at a later time, say $\Delta \gg 1$, by $\delta = |E(t+\Delta)-E(t'+\Delta)|$, which can be read from the time series. Then, if it is found that $\delta \simeq \delta_0 e^{\lambda\Delta}$, the largest Lyapunov exponent is determined by

$$\lambda = \frac{1}{\Delta} \lim_{\delta_0 \to 0} \ln\left(\frac{\delta}{\delta_0}\right). \tag{5}$$

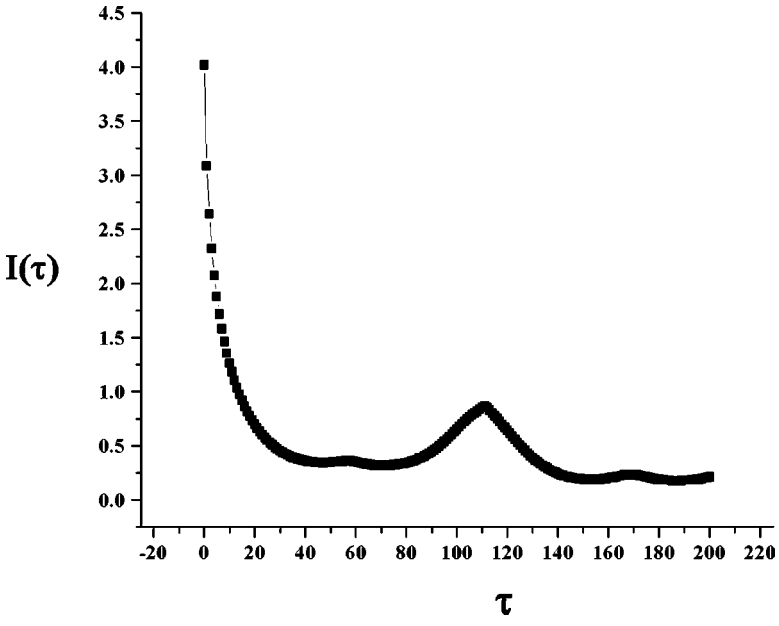

FIG. 12. Mutual information method applied to the data used in reconstructing the attractor shown in Fig. 11. Compare to Fig. 5.

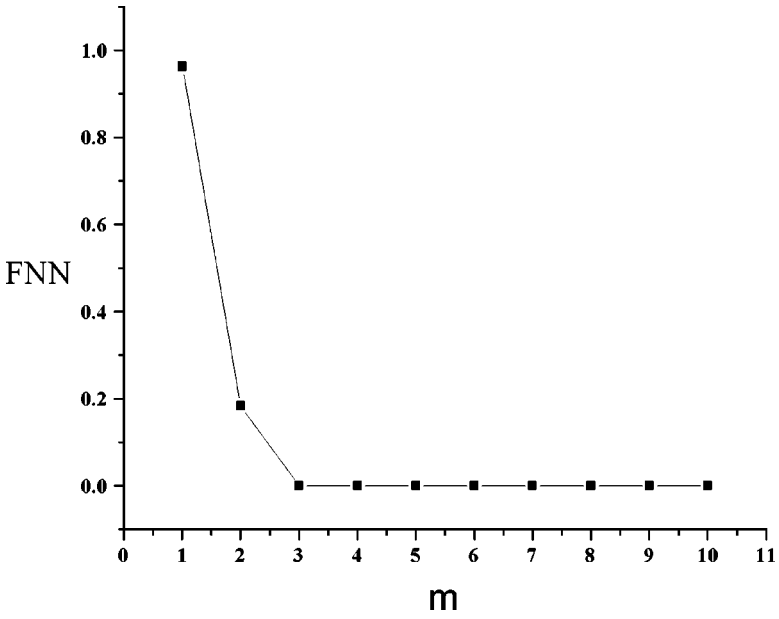

FIG. 13. Number of false neighbors as a function of the embedding dimension m for the attractor shown in Fig. 11.

If λ is positive, this means an exponential divergence of nearby trajectories, i.e., chaos. In practice, there will be fluctuations due to many effects[16] but it is possible to derive a consistent, and unbiased estimator of the largest Lyapunov exponent by computing

$$S(\epsilon,m,t)=\left\langle \ln\left(\frac{1}{|U_n|}\sum_{E(t')\in U_n}|E(t+\Delta)-E(t'+\Delta)|\right)\right\rangle, \tag{6}$$

where U_n is a neighborhood of $E(t)$ with diameter ϵ, and the angular brackets denote an average over both, different ϵ values and minimal embedding dimension m_0. If $S(\epsilon,m,t)$ exhibits a linear increase with identical slope for all $m>m_0$, and for a reasonable range of ϵ, then this slope can be taken as an estimate of the maximal exponent λ. For our particular case, different values for m_0 (from 2 to 5) were used and averaged; however, since the previous analysis had given three as the exact embedding dimension, and the averaged result did not differ from this particular curve, we only present the result with this single value. Also, the routines used for the calculations (Ref. 14) use five values for ϵ that are automatically generated from the time series data.

Figure 8 shows the value of the largest Lyapunov exponent for the oscillator in site 21 calculated via the method briefly sketched earlier (described in detail in Ref. 14).

Values for the largest Lyapunov exponents at the two stages where the breather stops are given in Table I; the time delay used in the analysis is the same for both resting stages ($\tau=50$).

The fact that all first Lyapunov exponents are positive confirms the chaotic character of the system dynamics. Since a larger positive value for the first Lyapunov exponent implies a faster divergence in time for states initially close to each other, one can see from the values in Table I that this divergence is less strong for the second stop in comparison to the first one. One could say that the localized mode is becoming less chaotic with time, in agreement with the exponential decay (with enormous time constants) found in Ref. 10.

IV. BREATHERS IN MOTION

Since the breather has not completely formed during the first moving stage, i.e., the energy is still dispersed in several sites, the computation of the interesting values becomes very complicated and inaccurate. Therefore, we only analyze the second moving stage: $t\in[1470,1895]$, when most of the energy is concentrated in the moving breather. Note that during this lapse, there is some energy that simultaneously travels to the left of the array, bounces back at sites 3 and 4, and collides with the moving breather just before it stops again (Fig. 1).

For the analysis of the moving energy, one has to set a threshold value in order to decide when the breather has left a site and moved to the next one in the sense of its motion. This allows for the individualization of the energy values that form the time series of the moving breather. The threshold value used is only determined by the two sites that form the heart of the breather, and corresponds to half the value of the energy in the breather at a particular site, i.e., when the energy in a site (say site 21) decreases to less than half its initial value (energy in site 21 when breather is at rest in sites 20–23), one then considers that the breather has moved from such site (21) and takes the value of the energy in the following site in the sense of the motion (site 22 in our example). The energy contained in the two central moving sites of the breather does not decrease considerably during the lapse it remains in motion and constitutes, therefore, a reliable indicator of its presence.

Figures 9–14 show the results of the analysis; the similarity with the results obtained for the resting breather is striking. The characterization of the moving breather with the discussed tools indicates a behavior that is remarkably

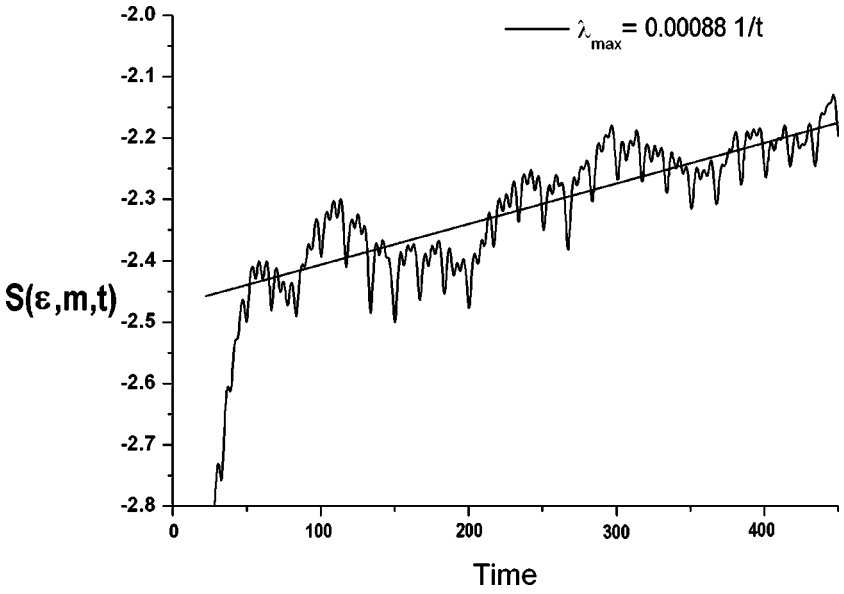

FIG. 14. Largest Lyapunov exponent for the center of the breather represented as a time series in Fig. 9. Compare to Fig. 8 and the values in Table I.

similar to the behavior of the breather at rest; comparing these figures to those in Sec. III, several deductions can be made.

Starting with Figs. 2 and 9, it can be observed that there is a decrease in the amplitude of the oscillators in the center of the breather as time increases, and that this shrinkage also reduces its value with time; this is consistent with the fact that the breather evolves under the influence of all the oscillators in the system.

From Figs. 3 (upper panel) and 10 one observes that the highest frequency $(\omega_3/2\pi)$ is now playing a more important role than the intermediate one $(\omega_2/2\pi)$, an interchange that remains for the next stop of the breather, Figure 3 (lower panel); recall Sec. III A. This is also clear in Figs. 6 and 11 where the interchange in the roles played by $(\omega_3/2\pi)$ and $(\omega_2/2\pi)$ is responsible for the modification in the form of the attractor. Figures 6 and 11 also show that the region occupied by the attractor is shrinking with time, i.e., the breather continues participating of the collective dynamics and losing energy via interactions with other modes still present in the system, mainly while in motion; the energy lost by the breather will in turn be dissipated at the end-sites of the array.

Figures 5 and 12, on the one hand, and Figs. 7 and 13, on the other, confirm that the time delay chosen is an optimal value, and that the immersion dimension is strictly three for both states of the breather, at rest or in motion; this, in conjunction with the other findings already mentioned, partly explains the similar behavior during both states.

Finally, even though the value of the first Lyapunov exponent for the moving breather is smaller than its value when the breather is at rest, it remains positive $(0.000\,88 \pm 0.000\,15)$, confirming that the analyzed breather, either at rest or in motion, is indeed a chaotic system.

V. DISCUSSION

It has been shown that the analysis and tools employed for time series and state reconstruction of a dynamical system are also very useful for the detection and characterization of spontaneously appearing breathers in thermal nonlinear arrays. All the calculations performed for the example analyzed in detail, agree and confirm the results previously found for the dynamics of the system.[10] This specific detailed case constitutes an example of systems whose chaotic behavior is governed by a small number of incommensurable frequencies, a situation reminiscent of the mechanism proposed by Ruelle and Takens for the appearance of chaotic behavior.

The usefulness of the analysis is of particular importance in experimental situations where the local energy (or a similar local variable) is the only quantity that may be precisely measured as a function of time. We thus propose the use of the analysis and tools described in the previous lines as a reliable method (probably the easiest one) for the study of nonlinear experimental situations where one suspects that the ubiquitous breathers might be present. The recent experimental detection of localized modes in an antiferromagnetic spin lattice[17] could provide another example for the application of the analysis just described.

ACKNOWLEDGMENTS

A.A.C. acknowledges financial support from UNAM and CoNaCyT, and J.R.C. from CoNaCyT, both during the realization of the work presented here.

[1] E. Hopf, Commun. Pure Appl. Math. **1**, 303 (1948).
[2] L. Landau and E. Lifshitz, *Fluid Mechanics* (Pergamon, Oxford, 1959).
[3] D. Ruelle and F. Takens, Commun. Math. Phys. **20**, 167 (1971).
[4] S. Newhouse, D. Ruelle, and F. Takens, Commun. Math. Phys. **64**, 35 (1978).
[5] A. Brandtl, T. Geisel, and W. Prettl, Europhys. Lett. **3**, 401 (1987); C. van Atta and M. Gharib, J. Fluid Mech. **174**, 113 (1987); A. Kourta, H. C. Boisson, P. Chassaing and H. Ha. Minh, *ibid.* **181**, 141 (1987).
[6] J. Gollub and S. Benson, J. Fluid Mech. **100**, 449 (1980); R.W. Walden, Paul Kolodner, A. Passner, and C. M. Surko, Phys. Rev. Lett. **53**, 242 (1984).
[7] C. Grebogi, E. Ott, and J. Yorke, Phys. Rev. Lett. **51**, 339 (1983); Physica D **15**, 354 (1985).
[8] P. S. Linsay and A. W. Cumming, Physica D **40**, 196 (1989).
[9] R. Reigada, A. Sarmiento, and K. Lindenberg, Phys. Rev. E **64**, 066608 (2001).

[10]R. Reigada, A. Sarmiento, and K. Lindenberg, Chaos **13**, 646 (2003).
[11]T. Cretegny, T. Dauxois, S. Ruffo, and A. Torcini, Physica D **121**, 109 (1998).
[12]R. Reigada, A. Sarmiento, and K. Lindenberg, Physica A **305**, 467 (2002).
[13]R. Reigada, A. Sarmiento, and K. Lindenberg, Phys. Rev. E **66**, 046607 (2002).
[14]H. Kantz, and T. Schreiber, *Nonlinear Time Series Analysis* (Cambridge University Press, Cambridge, UK, 2002); R. Hegger, H. Kantz, and T. Schreiber, Chaos **9**, 413 (1999) (http://www.mpipks-dresden.mpg.de/ãtisean.
[15]A. M. Fraser and H. L. Swinney, Phys. Rev. A **33**, 1134 (1986).
[16]H. Kantz, Phys. Lett. A **185**, 77 (1994).
[17]M. Sato and A. J. Sievers, Nature (London) **432**, 486 (2004).